European Congress on Computational Methods
in Applied Sciences and Engineering (ECCOMAS 2012)
J. Eberhardsteiner et.al. (eds.)
Vienna, Austria, September 10-14, 2012

UNSTEADY SIMULATIONS OF FLOW AND HEAT TRANSFER IN A PLANE TURBULENT IMPINGING JET USING URANS, DES AND LES

Rabijit Dutta[1], Anupam Dewan[2] and Balaji Srinivasan[3]

[1] Indian Institute of Technology Delhi
Department of Applied Mechanics
New Delhi – 110016, India
e-mail: rabijit13@gmail.com

[2] Indian Institute of Technology Delhi
Department of Applied Mechanics
New Delhi – 110016, India
e-mail: adewan@am.iitd.ac.in

[3] Indian Institute of Technology Delhi
Department of Applied Mechanics
New Delhi – 110016, India
e-mail: balaji.srinivasan@gmail.com

Keywords: Jet Impingement, Unsteady RANS equations, Detached Eddy Simulation and Large Eddy Simulation.

Abstract. *Unsteady Reynolds-Averaged Navier–Stokes (URANS) computations, Large Eddy Simulation (LES) and Detached Eddy Simulation (DES) of turbulent slot jet impingement have been performed at a Reynolds number of 13500 and H/d ratio of 10. Comparisons have been made in predicting the fluid flow and heat transfer characteristics with these different approaches. The predictions using steady RANS equations were also compared with URANS solutions and it was found that the predictions using URANS equations are in good agreement with the experimental data and are more accurate than the predictions using the steady RANS equations. Further, it was found that the latest version of the k–ω model shows much better agreement with the experimental data compared to that by the SST k–ω model. The surface Nusselt number distribution plot shows that both URANS equations with the latest version of the k–ω model and LES are capable of predicting the Nusselt number in the stagnation region, however, these are unable to accurately predict heat transfer in the region away from the stagnation point.*

1 INTRODUCTION

The high heat transfer rate of jet impinging flow has led to its wide industrial applications for cooling, heating and drying of surfaces, e.g., cooling of electronic equipment and turbine blades, drying of paper, and baking, freezing and drying of food products. Further, flow structures in the natural phenomenon of atmospheric microburst, which affects aircrafts and earth structures, are similar to impinging jet flow. Furthermore, fundamental understanding of the impinging flow is required for proper design of vertical take-off and landing (VTOL) aircrafts, which generate lift by impinging two jets into the ground during the take-off.

In addition to its various industrial applications and general practical relevance, its complex fluid flow structures comprising of a free-shear region, a stagnation region and wall jet regions (as shown in Figure 1) makes jet impingement flow a widely used benchmark case for the assessment of different Reynolds-Averaged Navier-Stokes (RANS) equations based turbulence models and subgrid scale models for Large Eddy Simulation (LES).

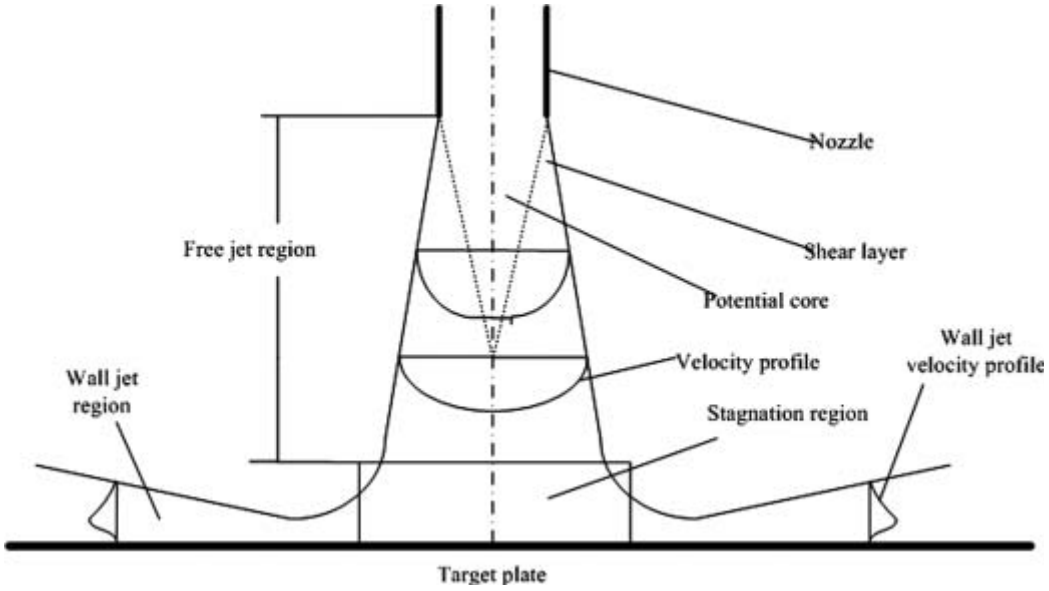


Figure 1: Flow structure in a jet impingement flow.

Because of its numerous fundamental as well as industrial applications, jet impinging flow has received significant attention from the researchers recently. These include both computational and experimental investigations of a slot jet as well as a circular jet impingement. Among some of the notable experimental studies on slot jet impinging flows, Gardon and Akfirat [1] studied the effects of turbulence on heat transfer characteristics of an impinging jet for various nozzle to plate distances and Reynolds numbers, Tu and Wood [2] measured wall shear stress and mean wall surface pressure at different Reynolds number and nozzle to plate spacings. Ashforth-Frost *et al*. [3] studied velocity and turbulence characteristics of a semi-confined jet at a Reynolds number of 20000 with various nozzle-to-plate distances. Maurel and Solliec [4] performed both flow visualization and flow measurements in an impinging jet to understand which parameters influence mass transfer.

Generally, computations of impinging flows are performed either to gain fundamental insight of the structures of the flow or to validate a computational model, which could be further useful for designing complex jet impinging systems. Fundamental investigations require the three-dimensional instantaneous flow field and therefore, direct numerical simulation (DNS) and large eddy simulation (LES) are the obvious choices. Beaubert and Viazzo [5] performed

LES using the dynamic sub-grid scale (SGS) model to study the influence of Reynolds number on the flow and heat transfer structures of an impinging slot jet at Reynolds numbers of 3000 and 7500. Tsubokura *et al.* [6] compared eddy structures for both slot and circular impinging jets at a Reynolds number of 6000 using LES. Hattori and Nagano [7] performed DNS using second order time and space discretization schemes at a Reynolds number of 9120 to understand the flow and heat transfer characteristics of a confined impinging slot jet.

Design of impinging systems requires computations at a very high Reynolds number and, therefore, RANS based turbulence models, which provide the time-averaged flow field data in small computational time, are the optimal choice. A number of studies have been performed to assess the performance of different RANS based turbulence models for impinging flows. Zuckerman and Lior [8] reviewed a few of these studies to compare the accuracy in predicting Nusselt number distribution of impinging flows by different RANS based turbulence models and concluded that of all turbulence models, $\overline{v^2} - f$ model and the SST k–ω model were the best in predicting both secondary peaks in the Nusselt number and the surface Nusselt number distribution. Generally, RANS based turbulence models lack generality in predicting impinging flows, in that a model may not give the same order of accuracy under a change of parameters. Further some models are too inaccurate to be useful at all. Dewan *et al.* [9], in their review paper, pointed out that some reasons for poor predictions by different turbulence models are flow complexity in the stagnation region, a large number of arbitrary coefficients inherent in these models, poor performance of the wall and damping functions and the way time averaging is performed. Recent studies reveal unsteadiness in the flow and heat transfer in impinging flows due to quasi-periodic impingement of large scale coherent structures in the impingement wall.

Hadziabdic and Hanjalic [10] reported that the secondary peak in the Nusselt number is associated with the formation of secondary vortices at the impingement wall and the corresponding unsteadiness in the flow. Therefore, it is hoped that the Unsteady RANS (URANS) equations, which are being widely solved to capture large scale unsteadiness in bluff body flows, can accurately predict the unsteady structures and consequently the secondary peak in the Nusselt number at a minimal cost compared to LES and DNS. Recently, Le Song and Prud'homme [11] performed URANS computations, to predict the coherent structures in jet impinging flows at a very small computational cost compared to LES and DNS at Reynolds number of 6000. However, they did not report the surface Nusselt number distributions. Kubacki and Dick [12] have already shown that the latest version of the k–ω model [13], with the inclusion of the stress limiter term in the definition of the eddy viscosity and the cross-diffusion term in the equation of specific dissipation rate, can accurately predict the flow and heat transfer in the stagnation region of a circular impinging jet. Subsequently Kubacki and Dick [14] used the same k–ω model in their hybrid RANS/LES simulations of plane impinging jet.

The objective of the present study is to perform URANS computations, DES and LES simulations of a 3D plane turbulent impinging jet under the same conditions and at the same mesh size and compare the advantages and disadvantages of all the three methods, in terms of accuracy in prediction of the fluid flow and heat transfer behavior. Some of the steady RANS solutions have also been presented here to check the usefulness of URANS computations over the steady RANS computations. Section 2 presents the governing equations and turbulence models used, Section 3 presents the details of flow configuration and boundary conditions, and Section 4 presents results followed by conclusions in Section 5.

2 COMPUTATIONAL METHODOLOGY

In this section governing equations and the solution methodologies used in the present paper are presented. The commercial finite volume based CFD package FLUENT 6.3.26 was used for numerical solutions of the governing equations and the mesh was generated using the commercial software GAMBIT 2.4.6.

2.1 Governing differential equations and solution parameters

2.1.1 Steady and unsteady RANS

In the steady RANS computations, incompressible time-averaged Navier-Stokes equations were computationally solved. The URANS equations considered were the same as the steady RANS equations with the only difference that the transient term was retained in the former. The URANS computations are widely used for flows with large scale unsteadiness. In the present study, four different turbulence models were considered for the steady RANS solutions, namely, the standard *k-ε* model with the standard wall functions, the standard *k-ε* model with the enhanced wall functions, the latest version of the *k–ω* model and SST *k–ω* model. Further, for the comparison of steady and unsteady RANS computations, the latest version of the *k–ω* model and SST *k–ω* model were considered. The latest version of the *k–ω* model was implemented into the FLUENT 6.3.26 solver by incorporating the equations through User Defined Functions (UDF). The governing equations used in the latest version of the *k–ω* model [13] are

$$\frac{\partial k}{\partial t} + \frac{\partial}{\partial x_j}\left(\overline{u_j} k\right) = P_k - \beta^* k\omega + \frac{\partial}{\partial x_j}\left[\left(\vartheta + \sigma^* \frac{k}{\omega}\right)\frac{\partial k}{\partial x_j}\right] \quad (1)$$

$$\frac{\partial \omega}{\partial t} + \frac{\partial}{\partial x_j}\left(\overline{u_j} \omega\right) = \alpha \frac{\omega}{k} P_k - \beta \omega^2 + \frac{\partial}{\partial x_j}\left[\left(\vartheta + \sigma \frac{k}{\omega}\right)\frac{\partial \omega}{\partial x_j}\right] + \frac{\sigma_d}{\omega}\frac{\partial k}{\partial x_j}\frac{\partial \omega}{\partial x_j} \quad (2)$$

Here, P_k represents the production of turbulent kinetic energy. The turbulent viscosity υ_t is defined as

$$\vartheta_t = \frac{k}{\overline{\omega}}\,, \overline{\omega} = \max\left(\omega, C_{lim}\sqrt{\frac{2\bar{S}_{ij}\bar{S}_{ij}}{\beta^*}}\right) \quad (3)$$

With the model constant $C_{lim} = 7/8$. The latest version of the *k–ω* model includes two extra terms compared to the earlier version of the *k–ω* model, namely, the stress limiter in the definition of the eddy viscosity, $C_{lim}\sqrt{\frac{2\bar{S}_{ij}\bar{S}_{ij}}{\beta^*}}$, and the cross diffusion term, $\frac{\sigma_d}{\omega}\frac{\partial k}{\partial x_j}\frac{\partial \omega}{\partial x_j}$, in the equation for ω. The stress limiter term makes it capable of predicting the flow in an impingement region, which is characterized by high levels of strain.

For both steady and unsteady RANS computations, all the equations were discretized using the second order upwind scheme for convective term and second order implicit scheme for time marching. For the pressure velocity coupling, SIMPLE algorithm was used for steady RANS and PISO scheme was used for unsteady RANS computations. A time step of 0.001 s was chosen for URANS simulations and in a single time step, all the equations converged to a residual of 10^{-5} within 20-25 iterations.

2.1.2 LES

For LES computations, Navier-Stokes equations were filtered such that eddies which are larger than the size of the filter are resolved and the ones smaller than the filter size are modeled. Generally, the size of the computational grid is used as a filter and the model for computing smaller scales is called the sub-grid scale (SGS) model. In the present work, the dynamic Smagorinsky model was used as the SGS model. This model dynamically calculates the value of Smagorinsky constant (C_s) based on the resolved scales of motion. For LES method, the bounded central difference scheme was used for the discretization of momentum equations and for the pressure-velocity coupling, PISO scheme was used. Time step was chosen to be 1×10^{-5} s and the solution took 10-15 iterations to converge in a single time step.

2.1.3 DES

In the DES approach, URANS equations are solved near the solid wall while LES equations are employed away from the wall [15]. FLUENT 6.3.26 has three versions of DES approach, depending on the URANS model it uses, namely, Spalart-Allmaras model, realizable k-ε model and SST k-ω model. In the present work DES based on SST k-ω model was used, where the dissipation term in the k equation is designed such that it changes to a LES model as the grid size becomes smaller than the turbulent length scale.

For the disctretization of the SST k-ω model, the second order upwind scheme was used. For the pressure-velocity coupling, PISO scheme was used and an optimal time step of 5×10^{-5} s was chosen based on the number of iterations required for the solution to converge in a single time step.

For all the unsteady simulations, it was observed that the flow becomes statistically steady at about 0.3 s to 0.4 s flow time. Therefore, data sampling, for calculating the statistics, was started after running the computations for 0.5 s and the statistics were calculated by averaging over next duration of 0.5 s.

3 FLOW CONFIGURATION AND BOUNDARY CONDITIONS

The flow geometry with the boundary conditions has been shown in Figure 2. The domain extends 80 nozzle diameters (d) in the x-direction, which is enough to use pressure outlet boundary condition at the outlet of the domain [14], and in the z–direction domain size was 3.14 nozzle diameters (d), which was recommended by different researchers for using periodic boundary conditions as reviewed by Dewan *et al*. [9]. The boundary conditions are also shown in Figure 2. For all the simulations, a mesh similar to the one used by Kubacki and Dick [14] was used here. The mesh contained 1.1 million grid points with a large number of elements placed near the walls and the jet shear-layers.

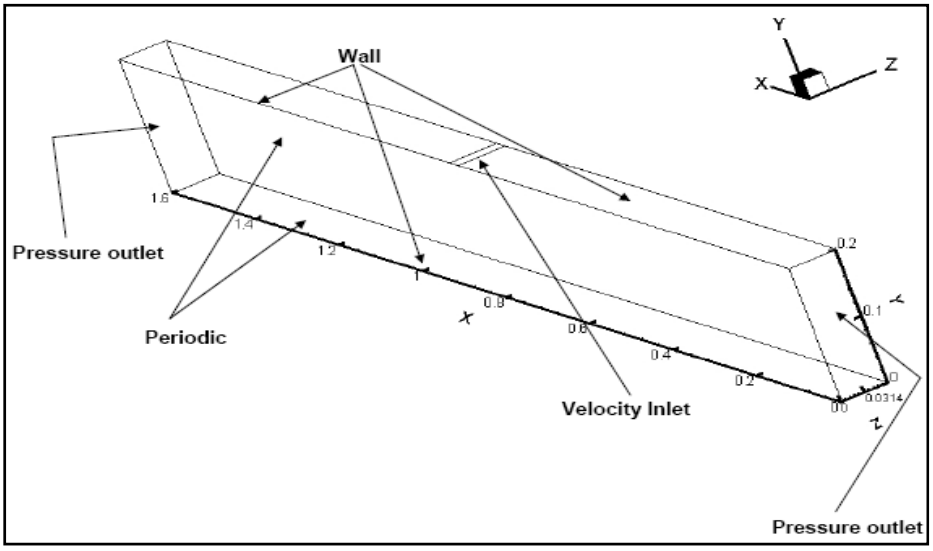


Figure 2: Flow geometry and boundary conditions.

At the nozzle outlet, a velocity profile was specified which resembled the velocity profile measured by Maurel and Solliec [4] and is given as $V = V_O [1 - (x/B)^{14}]$. Here, V_O denotes the centerline velocity and B the width of the slot jet. The no-slip boundary conditions were specified at the confinement as well as the impingement plates. At the outlet, atmospheric pressure was specified and in the transverse direction (z-direction) periodic boundary conditions were specified to reduce the size of the domain in that the z-direction. Further, at the nozzle outlet, constant profiles of k and ω were specified for RANS and DES calculations based on earlier observations [14]. The spectral synthesizer technique was used for LES to generate turbulence at the inlet. In this method, a divergence free velocity vector field is synthesized in the Fourier space to generate fluctuating velocity components.

For solving the energy equation, a constant temperature $T_w = 310$ K was specified at the impingement wall and at the inlet a temperature $T_i = 300$ K was specified. For the confinement walls, the adiabatic condition was used.

4 RESULTS AND DISCUSSION

4.1 Flow behavior

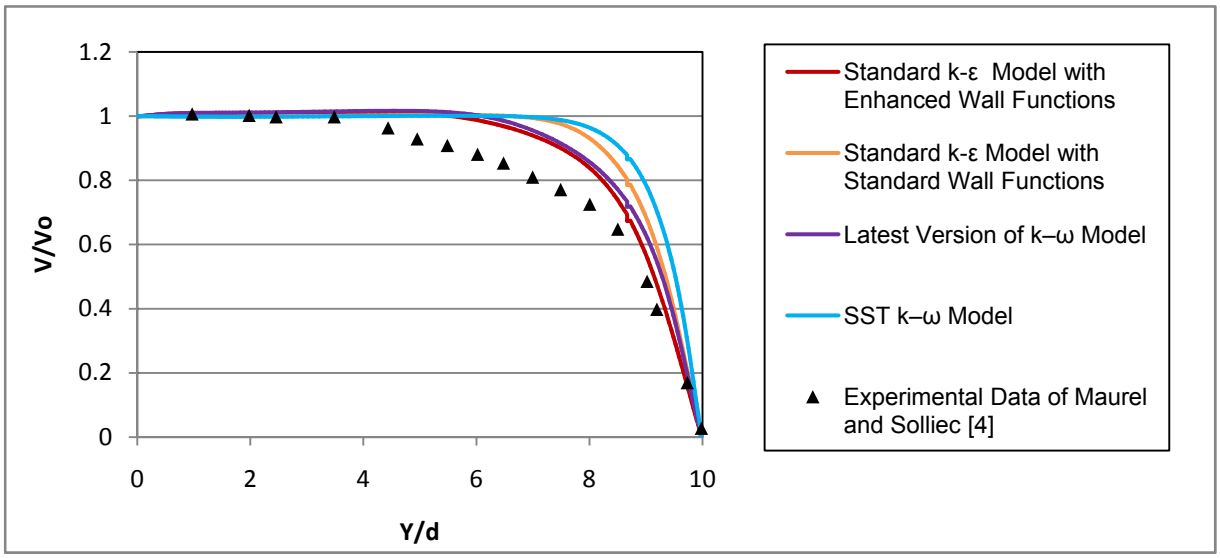
In this section, results of flow behavior have been presented for different modeling approaches. The predicted mean and fluctuating velocities in the y-direction along the jet centerline and skin friction coefficient along the impingement wall were compared with the experimental results reported in the literature [2, 4]. Initially, comparisons have been made between different steady RANS models. Subsequently steady and unsteady RANS solutions have been compared and finally results of URANS, LES and DES computations are also compared.

4.1.1 Comparison of different steady RANS equations based turbulence models

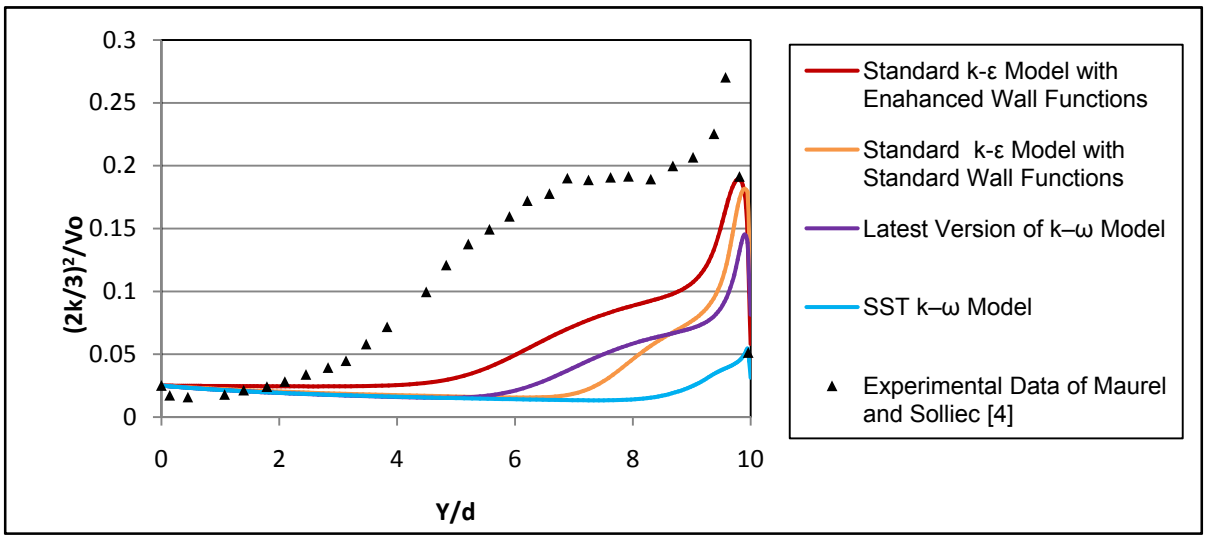
As already mentioned, the periodic impingement of the secondary vortices make the flow unsteady, however, steady RANS solutions may have the capability to capture all the flow complexities, except unsteadiness. Hence here we assess the performance of different turbulence models in computing impinging flows. As expected, the mean velocity comparisons

show that the potential core is highly overpredicted by all the models [Figure 3 (a)]. Further, none of the RANS based turbulence models are able to capture the fluctuating y-velocity along the jet centerline [Figure 3 (b)]. Compared to other models, the latest version of *k-ω* model and the standard *k-ε* model with enhanced wall functions are able to accurately predict the trend in the skin friction coefficient along the impingement plate [Figure 3 (c)].

(a)



(b)



(c)

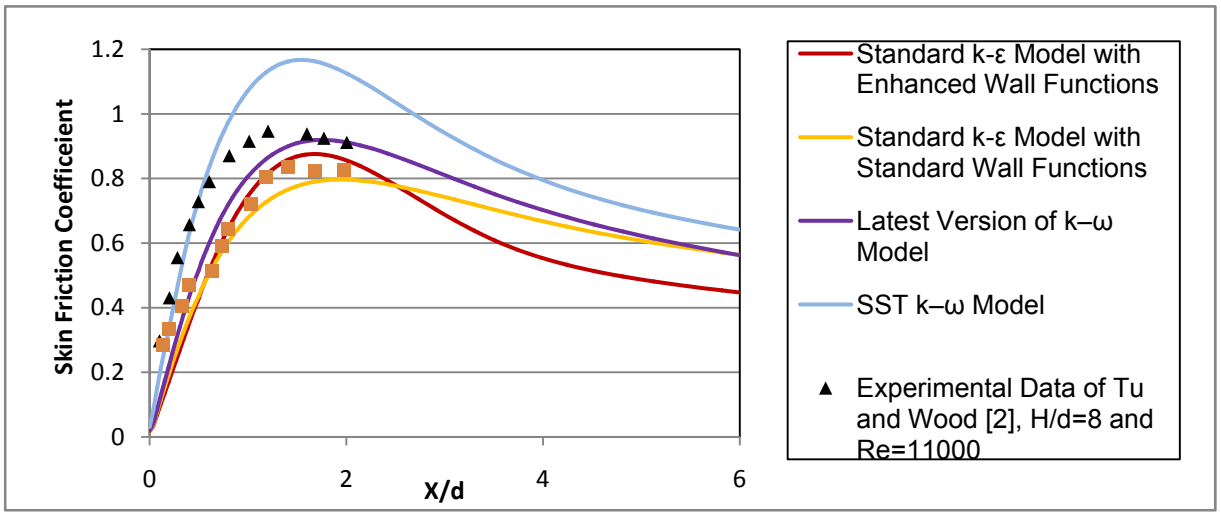
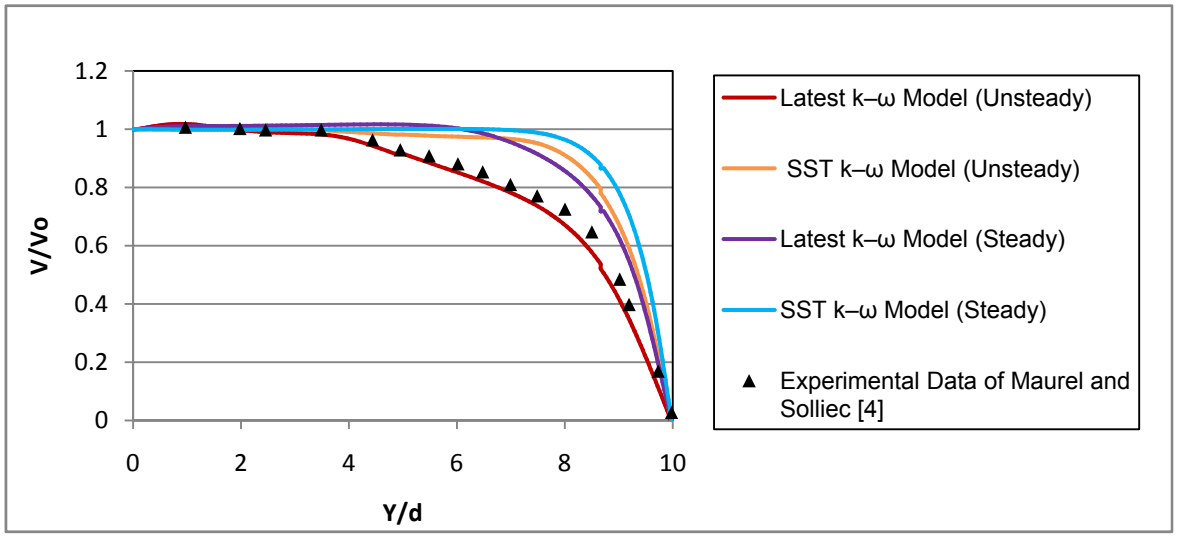


Figure 3: Comparisons of different steady RANS models (a) mean velocity along the centreline of the jet (b) fluctuating y-velocity along the centreline of the jet (c) skin friction coefficient along the impingement plate.

4.1.2 Comparison of steady and unsteady RANS computations

Figure 4 shows a comparison of steady and unsteady RANS computations in predicting flow behavior in the impinging flow. The unsteady RANS equations show a substantial improvement over the steady RANS equations in predicting the mean normal velocity along the jet centreline, especially, the mean velocity predictions form the URANS computations using the latest version of the *k–ω* model show a good agreement with the experimental data. Further, Figure 4 (b) shows that the skin friction coefficeint predicted by URANS equations with the *k–ω* model shows a trend similar to the experimental data. However, it could not be quantified as there was no experimental data available at Re = 13500 and H/d = 10 considered in the present study.

(a)



(b)

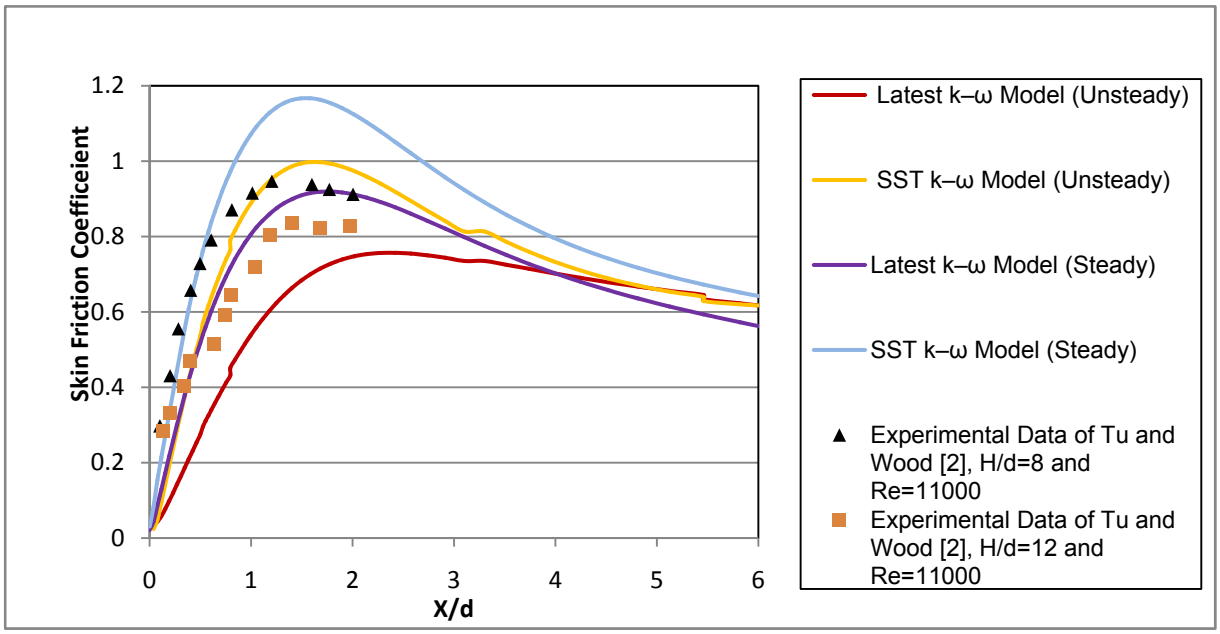


Figure 4: Comparisons between steady and unsteady RANS models (a) mean velocity along the centreline of the jet (b) skin friction coefficient along the impingement plate.

4.1.3 Comparisons of URANS, DES and LES computations

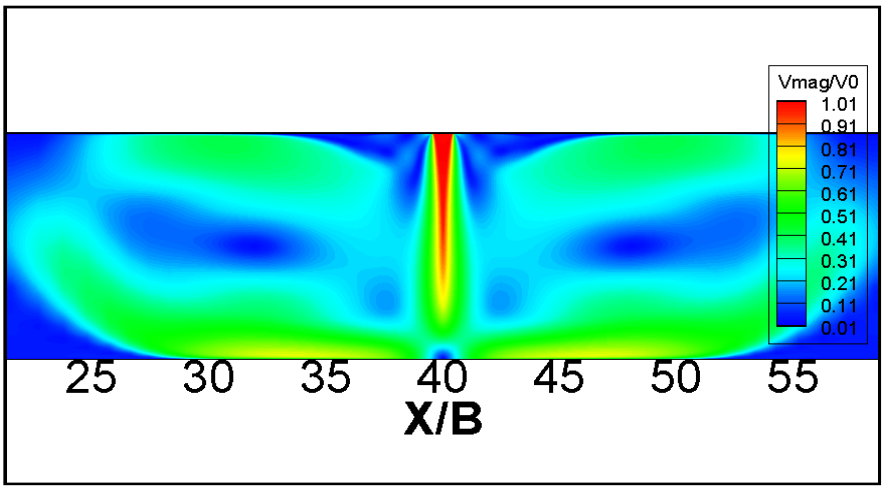
4.1.3.1 Computational time requirement

The computational time required to run the simulations for a flow time of 0.5 s in a system of 8 processors with parallel processing and with 8 GB of RAM was approximately 8 days for LES and approximately 5 days for DES, while it took approxiametly 30 hours for URANS simulations. Therefore, in terms of the computational cost, URANS simulation is quite advantageous than LES and DES computations.

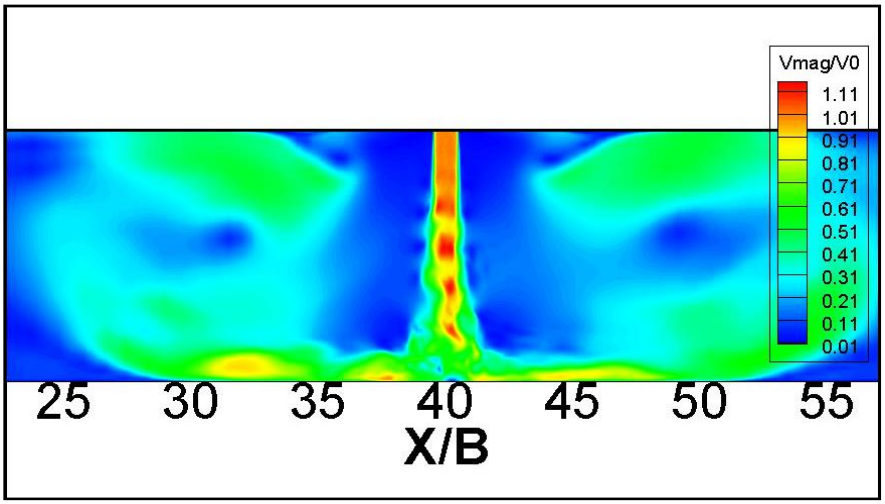
4.1.3.2 Comparison of instantaneous velocity contours

Figure 5 shows a comparison of instantaneous velocity contours between URANS, DES and LES computations at flow time of 0.3 s. It can be clearly seen that the overall picture of the DES and LES computations are quite similar and much more detailed, in terms of flow structures, compared to the corresponding URANS computations. Further, it qualitatively shows that the LES computations have well resolved different scales of turbulence, while URANS computations are not able to show the range of turbulence eddy structures.

(a)



(b)



(c)

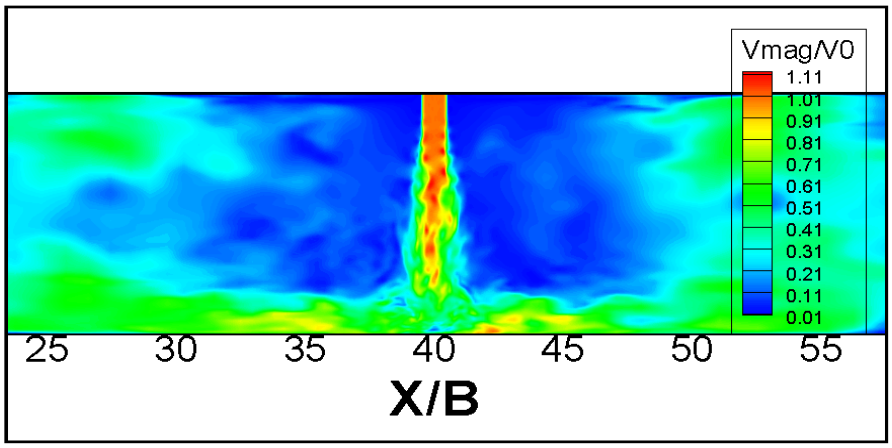


Figure 5: Comparisons of instantaneous velocity contours from (a) URANS, (b) DES and (c) LES.

4.2 Heat transfer characteristics

4.2.1 Comparison of surface Nusselt number distribution for steady and unsteady RANS computations

Figure 6 shows the Nusselt number distributions at the impingement surface given by steady and unsteady RANS equations and by using latest version of k-ω model and SST k-ω model and their comparisons with the experimental data reported in the literature [16]. Since, no experimental data is available at the particular Re = 13500 considered in the present paper, quantitative estimates of the error cannot be made. However, it can be seen from Figure 6 that the unsteady RANS solutions using the latest version of the *k–ω* model provide the most accurate value of the Nusselt number in the region of impingement. All the models overpredict the value of the Nusselt number far away from the impingement region.

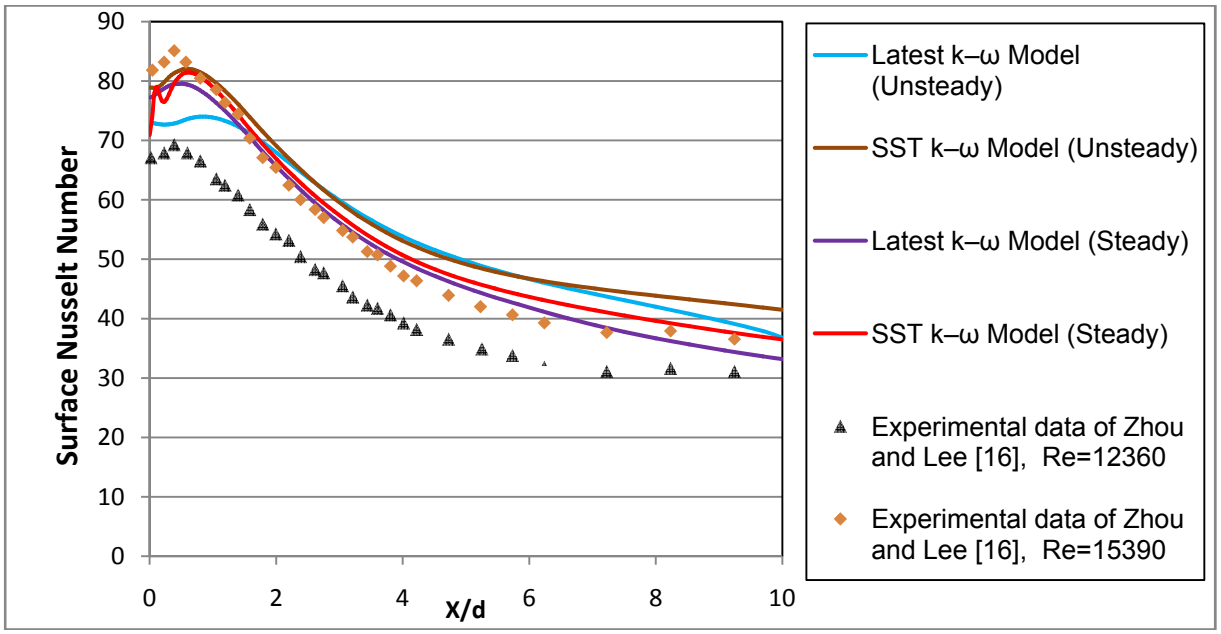


Figure 6: Nusselt number predictions from steady and unsteady RANS models.

4.2.2 Comparison of surface Nusselt number distribution for URANS and LES computations

Figure 7 shows that the Nusselt number at the impingement region predicted by LES and the URANS equations (by using the latest *k–ω* version of the model) are comparable to each other. At the regions far away from the stagnation point, LES shows a similar trend to the experimental results, however, it underpredicts the value of Nusselt number. This under prediction is probably due to the resolution of the mesh that is not suitable for the LES in those regions.

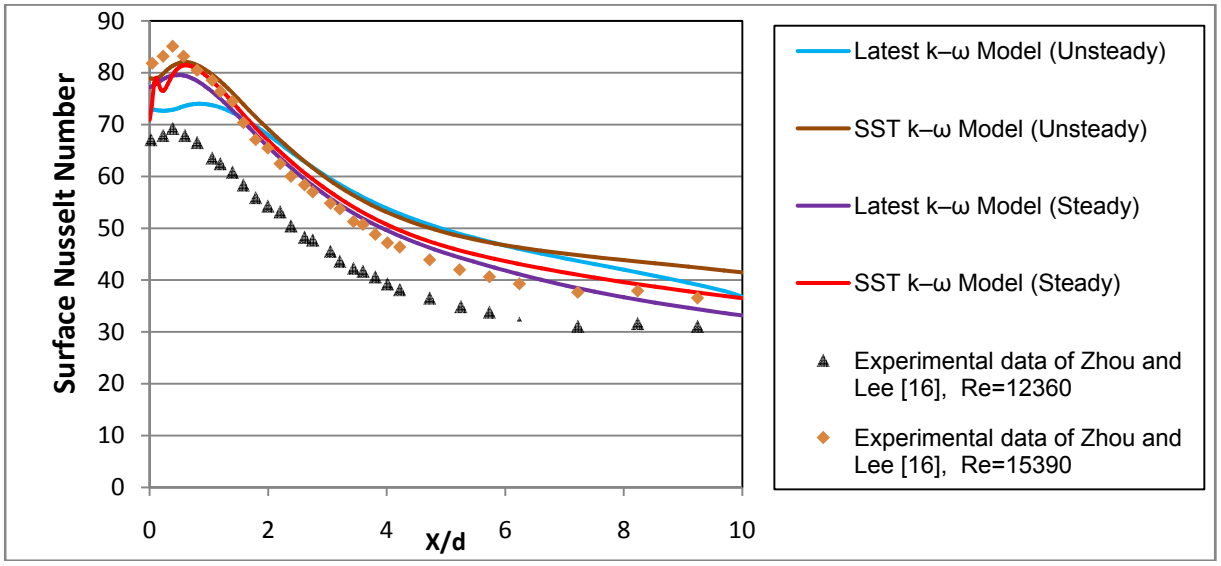


Figure 7: Nusselt number predictions from URANS and LES models.

5 CONCLUSIONS

In the present paper the performance of different turbulence models has been compared in predicting impinging flow. It has been observed that the steady RANS equations are not capable of predicting the behavior of turbulent jet impinging normally on a flat plate, because of the complexities involved in these kinds of flow. Further, it has been found that the URANS equations with the latest version of the *k-ω* model accurately predict flow properties. Comparisons have also been made between URANS, DES and LES computations. It is observed that LES is well capable of resolving the smallest scales of turbulence while it takes substantially higher computational time compared with DES and URANS. Further, Nusselt number distribution shows that both LES and URANS simulations can predict the stagnation Nusselt number and are incapable of accurately predicting Nusselt number away from the impingement region.

REFERENCES

[1] R. Gardon, J. C. Akfirat: The role of turbulence in determining the heat transfer characteristics of impinging jets. *International Journal of Heat and Mass Transfer*, 8 (1965), 1261-1272.

[2] C.V. Tu, D.H. Wood: Wall pressure and shear stress measurements beneath an impinging jet. *Experimental Thermal and Fluid Science*, 13 (1996), 364-373.

[3] S. Ashforth-Frost, K. Jambunathan, C.F. Whitney: Velocity and turbulence characteristics of a semi-confined orthogonally impinging slot jet. *Experimental Thermal and Fluid Science,* 14 (1997), 60-67.

[4] S. Maurel, C. Solliec: A turbulent plane jet impinging nearby and far from a flat plate. *Experiments in Fluids*, 31 (2001), 687-696.

[5] F. Beaubert, S. Viazzo: Large eddy simulations of plane turbulent impinging jets at moderate Reynolds numbers. *International Journal of Heat Fluid Flow*, 24 (2003), 512-519.

[6] M. Tsubokura, T. Kobayashi, N. Taniguchi, W.P. Jones: A numerical study on the eddy structures of impinging jets excited at the inlet. *International Journal of Heat and Fluid Flow*, 24 (2003), 500-511.

[7] H. Hattori, Y. Nagano: Direct numerical simulation of turbulent heat transfer in plane impinging jet. *International Journal of Heat and Fluid Flow*, 25 (2004), 749-758.

[8] N. Zuckerman, N. Lior: Jet impingement heat transfer: physics, correlations, and numerical modeling. *Advances in Heat Transfer*, 39 (2006), 565-631.

[9] A. Dewan, R. Dutta, B. Srinivasan: Recent trends in computation of turbulent jet imptngement heat transfer. *Heat Transfer Engineering*, 33 (2012), 447-460.

[10] M. Hadziabdic and K. Hanjalic: Vortical structures and heat transfer in a round impinging jet. *Journal of Fluid Mechanics*, 596 (2008), 221-260.

[11] G. LeSong and M. Prud'homme: Prediction of coherent vortices in an impinging jet with unsteady averaging and a simple turbulence model. *International Journal of Heat and Fluid Flow*, 28 (2007), 1125-1135.

[12] S. Kubacki and E. Dick: Convective heat transfer prediction for an axisymmetric jet impinging onto a flat plate with an improved k–ω model. *International Journal of Numerical Methods for Heat and Fluid Flow*, 19 (2009), 960-981.

[13] D.C. Wilcox: Turbulence modeling for CFD, La Canada, California, USA, 2006.

[14] S. Kubacki and E. Dick: Simulation of plane impinging jets with k–ω based hybrid RANS/LES models. *International Journal of Heat and Fluid Flow*, 31 (2010), 862-878.

[15] A. Dewan: Tackling turbulent flows in engineering, Springer, Germany, 2011.

[16] D.W. Zhou and S.-J.Lee: Forced convective heat transfer with impinging rectangular jets. *International Journal of Heat and Mass Transfer*, 50 (2007), 1916-1926.